I&EC research
Industrial & Engineering Chemistry Research
pubs.acs.org/IECR
Article

Active Solvent Hydrogen-Enhanced *p*-Nitrophenol Reduction Using Heterogeneous Silver Nanocatalysts@Surface-Functionalized Multiwalled Carbon Nanotubes

T. S. Swathy, M. Jinish Antony,* and Naijil George

Cite This: *Ind. Eng. Chem. Res.* 2021, 60, 7050−7064
Read Online

ABSTRACT: Solvent effects in aqueous media for the fast heterogeneous catalytic reduction of *p*-nitrophenol were studied using two silver nanocatalysts. Binary and ternary silver nanocatalysts (BNC and TNC) utilize functionalized multiwalled carbon nanotubes (MWCNTs) and polythiophene-functionalized MWCNT nanocomposites as hosts for silver nanoparticles, respectively. The catalytic reduction kinetics were measured by UV−visible absorption spectroscopy by observing the decrease of the sodium nitrophenolate ion peak at 400 nm. The first-order rate constants (k) obtained to reduce *p*-nitrophenol (1.0×10^{-4} M) in an aqueous medium using TNC and BNC by taking optimum nanocatalytic concentrations were 0.0134 and 0.0364 s^{-1}, with the activity factor 113.34 and 303.34 s^{-1} g^{-1}, respectively. The role played by each component of BNC and TNC nanocomposites was determined using control experiments. UV−visible (UV−vis) absorption spectroscopy, powder X-ray diffraction studies, and X-ray photoelectron spectroscopy (XPS) analysis on recycled catalysts have revealed no substantial deactivation in catalytical activity or loss of silver nanoparticles for recycled TNC up to the fifth cycle and for recycled BNC up to the sixth cycle. Field emission scanning electron microscopy (FE-SEM) analysis manifested the crystalline byproducts of sodium metaborate hydrates which could also decelerate catalytic activity in higher cycles. The relative rates of catalytic hydrogenation in different solvent−water mixtures indicated that a 10% glycerol−water mixture is a green and nontoxic solvent combination for accelerating the catalytic reduction of *p*-nitrophenol. The quantity of catalyst and sodium borohydride was minimized by employing a 10% glycerol−water mixture. The highest activity factor of 936.50 s^{-1} g^{-1} was achieved using the BNC nanocatalyst (0.005 mg/mL) with the P-NP to $NaBH_4$ molar ratio of 1:200. The catalytic reduction of *p*-nitrophenol in different solvent−water mixtures revealed that the reduction rate directly depends on the active hydrogen present in the solvent molecules. The industrial-scale reduction of concentrated *p*-nitrophenol (1.0×10^{-1} M) was achieved by the addition of $NaBH_4$ (25 times higher molar equivalent to P-NP) using a relatively low catalyst concentration (BNC-0.18) in a reasonable reaction time of 1 h. The ternary nanocatalyst (TNC) has shown stable dispersion in water than BNC, which is suitable as an excellent antibacterial agent for *Escherichia coli* bacteria cultured in water-based nutrient broth at a low concentration (10 μg/mL).

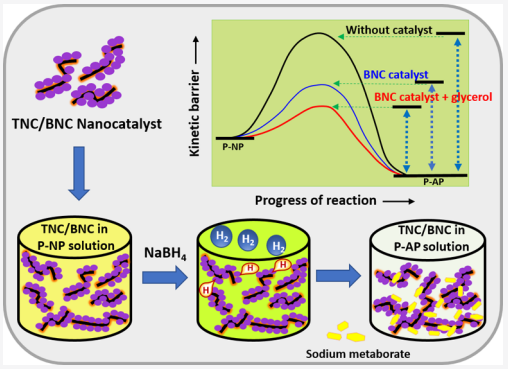

1. INTRODUCTION

Heterogeneous catalysis has tremendous applications in many organic transformations, as seen in many industrial and academic research studies.[1−7] Heterogeneous transition-metal nanocatalysts have attracted significant attention because of their mild reaction conditions, recyclability, enhanced catalytic performance, and simple separation strategies.[8−21] Among different transition-metal nanocatalysts, silver nanoparticles, in particular, possess special features such as ease of synthesis, good catalytic activity, remarkable electrical and optical properties, less toxicity, and cost effectiveness.[22−24] Silver nanoparticles could function as stable nanocatalyst for desired applications via stabilizing them with capping molecules, surfactants, and polymer matrices.[22,25,26] Heterogeneous catalysts have good prospect in recovery and reusability than homogeneous catalysts. However, the former inherently exhibits poor solubility/dispersibility.[27,28] Bare colloidal nanoparticles have an aggregation effect with time, reducing the catalyst activity with storage.[8,9] In addition to that, colloidal nanoparticles require a tedious process to be purified from the mother liquid, whereas heterogeneous catalysts can be purified by simple washing and filtration. The irreversible nature of homogeneous silver colloidal systems restricts its use to single catalytic use. Therefore, facile, green, and cost-effective metal nanoparticle-supported heterogeneous nanocomposites with

Received: April 10, 2021
Revised: April 16, 2021
Accepted: April 24, 2021
Published: May 10, 2021

https://doi.org/10.1021/acs.iecr.1c01371
Ind. Eng. Chem. Res. 2021, 60, 7050−7064

good dispersibility in water or other solvents deserve immense attention in recent times. Polymer/carbon nanomaterial-hosted metal nanocatalysts have been recognized as green catalysts because of the energy benefits in catalytic use and catalytic recyclability without significant loss of nanoparticles from the heterogeneous structure.[29,30] The nanocomposites of polyelectrolyte−carbon nanotube host system could provide good dispersibility, charged cationic or anionic side chains, and good mechanical stability.[30] Conducting polymers were recently used for the preparation of conducting polymer-multiwalled carbon nanotube (MWCNT) nanocomposites by in situ polymerization. Conducting polythiophene−MWCNT nanocomposites have high electrical conductivity, good optical properties, biocompatibility, environmental/thermal stability, and better host interactions with metal nanoparticles.[31] The stability of metal nanoparticles against oxidation, agglomeration, dispersibility, and leaching from the supporting framework remained as the critical issues to address for the performance of heterogeneous polymer/carbon nanomaterial-supported metal nanocatalysts.[28−35]

The catalytic reduction of *p*-nitrophenol using sodium borohydride as a hydride source in the presence of different nanocatalysts is considered as a typical model reaction because of mild reaction conditions, moderate reaction kinetics, and simple experimental setup.[36−38] The high reaction rate was not achieved until we use an excessive quantity of sodium borohydride to exhibit pseudo-first-order and more than the minimum quantity as a catalyst. The catalytic reduction of *p*-nitrophenol, therefore, requires some improvements in reaction conditions to obtain enhanced catalytic conversion with minimum reagents and catalysts. The acceleration of reaction kinetics with some metal salts or other reagents has been reported recently in the literature.[39−42] The mechanism of the catalytic reduction of *p*-nitrophenol for substantiating the actual source of hydrogen still remains to be ambiguous.[39,43−47] Recently, Zhao et al. investigated the catalytic reduction of *p*-nitrophenol with sodium borohydride using a deuterium isotope experiment. Their work substantiated the requirement of polar protic solvents, and it acts as the source of hydrogen rather than hydride reducer.[43] Fountoulaki et al. studied the kinetic isotope effects on the catalytic reduction of *p*-nitrophenol using $NaBH_4$ and $NaBD_4$, which has given evidence for B—H bond cleavage at the rate-determining step and the in situ formation of Au−H.[44] More validating evidence is required to understand the role of water and other protic solvents for the hydrogenation of *p*-nitrophenol.

The present work focuses on the reduction reaction of *p*-nitrophenol to *p*-aminophenol in the presence of ternary nanocatalyst (TNC) and binary nanocatalyst (BNC); both contain silver nanoparticles embedded on different hosts, polythiophene-functionalized MWCNT nanocomposites, and functionalized MWCNT, respectively. The kinetics of binary silver nanocatalyst (k = 0.0364 s^{-1}) were two to three times faster than the TNC (k = 0.0134 s^{-1}) at low *p*-nitrophenol concentrations. The optimum nanocatalyst concentration for reducing *p*-nitrophenol at 1 × 10^{-4} M concentration was determined to be 0.06 mg/mL. We have carried out reaction kinetics of nitrophenol in polar protic and aprotic solvents miscible with water. The glycerol−water mixture (5−30%) acts as the energizing solvent for nitrophenol reduction with $NaBH_4$. By employing a green solvent combination of 10% glycerol, the catalytic activity factor enhanced to 936.50 s^{-1} g^{-1} (three times higher activity than in water as the solvent); therefore, we could reduce the catalyst concentration and sodium borohydride concentration approximately to one-sixth. A plausible mechanism was demonstrated for the nitrophenol reduction using sodium borohydride and active hydrogens in the solvent. The ternary silver nanocatalyst showed better dispersion than the BNC, which led us to study the antimicrobial properties. The ternary nanocomposites with a lower atomic percentage of silver nanoparticles attached to the less cytotoxic polythiophene layer act as an efficient antibacterial agent against *Escherichia coli* bacteria.[48−50] In summary, the binary silver nanocatalyst functions as an efficient catalyst for reducing *p*-nitrophenol, whereas the ternary nanocatalyst acts as an excellent antibacterial material against *Escherichia coli* bacteria in solutions.[51−56]

2. EXPERIMENTAL SECTION

2.1. Materials and Reagents. Sodium borohydride was purchased from Sigma Aldrich. *p*-nitrophenol was purchased from LOBA chemicals. *p*-aminophenol was purchased from NICE chemicals. Acetone, glycerol (anhydrous), ethylene glycol, and 1,4-dioxane were purchased from Merck chemicals, India. Deionized water was used as a solvent in catalysis and nutrient broth preparation (a mixture of peptone, NaCl, and yeast extract from NICE chemicals and beef extract from Merck chemicals, India).

2.2. Measurements and Instruments. UV−vis absorption spectra of the samples were recorded by Shimadzu UV−visible spectrophotometer, UV 1800 series in the range 250−500 nm with deionized water. The powder wide-angle XRD of the samples was measured using PANALYTICAL, Aeris research with 2θ values ranging from 10° to 80°. FE-SEM and energy-dispersive X-ray (EDX) elemental mapping images were recorded using ZEISS ΣIGMA. The XPS analysis was conducted using PHI 5000 Versa Probe II, ULVAC-PHI Inc., USA X-ray photoelectron spectrometer. The optical densities of *E. coli*-inoculated samples were recorded in an antibacterial assay using an AU2701 UV−vis double beam spectrophotometer, systronics.

2.3. General Procedure. *2.3.1. Reaction Kinetics Using Different Nanocatalyst Concentrations.* Different concentrations of ternary silver nanocatalysts (TNCs) were prepared by dispersing 0.5, 1.0, 1.5, and 2.5 mg of TNCs in the *p*-nitrophenol solution (25 mL, 1.0 × 10^{-4} M) via sonication to obtain 0.02, 0.04, 0.06, and 0.10 mg/mL, respectively. The respective concentrations are abbreviated as TNC-0.02, TNC-0.04, TNC-0.06, and TNC-0.10, where the figures show the concentrations in mg/mL. Similarly, BNCs are designated as BNC-0.02, BNC-0.04, BNC-0.06, and BNC-0.10 for the same concentrations.

A typical procedure showed below to determine the reaction kinetics using nanocatalyst concentration TNC-0.06. The TNC (1.5 mg) was dispersed in *p*-nitrophenol (25 mL, 1.0 × 10^{-4} M) by sonication for 15 min. The freshly prepared $NaBH_4$ solution (2 mL, 1.0 × 10^{-1} M) was added to 2 mL of a sonicated mixture of *p*-nitrophenol and TNC (0.06 mg/mL) taken in a vial and shaken for 10 s. We have mixed the *p*-nitrophenol−nanocatalyst reaction mixture and sodium borohydride solution in equal volumes for all the catalytical studies, reducing the final concentrations of *p*-nitrophenol, sodium borohydride, and nanocatalyst equally to half (Table S1). UV−visible absorption spectra were recorded automatically in regular time intervals using the preset program. The

https://doi.org/10.1021/acs.iecr.1c01371
Ind. Eng. Chem. Res. 2021, 60, 7050−7064

UV−vis absorption spectra of *p*-nitrophenol reduction using different nanocatalyst concentrations TNC-0.02, BNC-0.02, TNC-0.04, BNC-0.04, BNC-0.06, TNC-0.10, and BNC-0.10 were recorded using the same reaction conditions (see the Supporting Information for procedure). The rate constants were calculated from the UV−visible absorbance of the final mixture.

2.3.2. Recycling Studies Using Nanocatalysts. TNC (7 mg) was dispersed in the *p*-nitrophenol solution (5 mL, 2.33×10^{-3} M) by sonication for 15 min. Freshly prepared $NaBH_4$ solution (5 mL, 2.33 M) was added to the above mixture. The reaction mixture was shaken well for 1 min, then kept undisturbed for 10 min, and centrifuged. After centrifugation for 3 min, the filtrate was decanted, and then, UV−visible absorption spectra were recorded. The residue (nanocatalyst) was washed with deionized water, and catalytical activities continued for four more consecutive cycles using the same method. A similar procedure was repeated using the BNC nanocatalyst (7 mg) instead of TNC for six catalytic cycles (see the Supporting Information).

2.3.3. Recycling Effects of Nanocatalysts on Morphology and Composition. The nanocatalyst TNC (25 mg) was dispersed in the *p*-nitrophenol solution (25 mL, 1.66×10^{-3} M) by sonication for 15 min. The freshly prepared $NaBH_4$ solution (25 mL, 1.66 M) was added and shaken well for 1 min to the above mixture. It was kept undisturbed for 10 min to complete the reaction and filtered. The nanocatalyst residue obtained was again dispersed in the *p*-nitrophenol solution (25 mL, 1.66×10^{-3} M) and the process was repeated up to the ninth cycle in the same manner. After the third, sixth, and ninth catalytic cycles, a portion (approximately one-third of the initial amount of catalyst) of the residue was separated and centrifuged to recover the catalyst. The residue was washed with water and acetone and then dried in a vacuum oven at 60 °C for 1 h. The morphology and composition of nanocatalysts were recorded using powder XRD, XPS, and SEM. The same procedure was repeated using the BNC nanocatalyst to find any difference in the morphology and composition (see the Supporting Information).

2.3.4. TNC-Catalyzed Reduction in Different Volume Percentages of Glycerol−Water Mixtures. TNC (1.5 mg) was dispersed in the *p*-nitrophenol solution (25 mL, 1.0×10^{-4} M) by sonication for 15 min. The $NaBH_4$ solution (5 mL, 1×10^{-1} M) prepared in different volume percentages of the glycerol−water mixture was added to the P-NP-TNC mixture (5 mL) taken in different vials. The final percentage volumes of glycerol in water were 5, 10, 20, 30, 40, and 50% v/v. The time for reaction completion was obtained from the change in color of the reaction mixture from greenish-yellow to colorless. The same procedure was repeated for the BNC catalyzed reduction of *p*-nitrophenol in different volume percentages of solvent mixtures. The other solvent mixtures such as ethylene glycol in water, ethanol in water, and 1,4-dioxane in water were similarly used as the solvent media for the catalytic reduction of P-NP using nanocatalysts. (see the Supporting Information).

2.3.5. Antibacterial Study Using TNC. Nutrient broth was prepared by dissolving NaCl (0.5%), peptone (0.5%), beef extract (0.3%), and yeast extract (0.3%) in double-distilled water. The pH was adjusted to 7.4 and sterilized by autoclaving at 15 lbs pressure (121 °C) for 15 min. The stock solution of dispersed TNC (200 μg/mL) was prepared in 50 mL nutrient broth by sonication for 30 min. Different concentrations of the TNC nanocatalyst such as 1×10^{-1}, 5×10^{-1}, 1, 5, 10, 20, 30, 40, 80, 120, and 160 μg/mL were prepared by adding 5, 25, 50, 250, 500, 1000, 1500, 2000, 4000, 6000, and 8000 μL of stock solution (200 μg/mL) to the nutrient broth to obtain 10 mL of total volume. The stock solution was also taken for antibacterial activity. Samples containing broth mixtures were sonicated for 10 min. All tubes were inoculated with 50 μL of actively growing *E. coli* culture and incubated overnight in a thermal shaker at 37 °C. After incubation, microbial growth in each tube was studied using a UV−visible double beam spectrophotometer by measuring the optical density at 660 nm. Positive and negative controls were used to validate the results.

3. RESULTS AND DISCUSSION

3.1. Comparison of TNC and BNC. Silver nanoparticles embedded TNC and BNC obtained by reducing the silver nitrate solution using ascorbic acid as a reducing agent. Polythiophene-functionalized MWCNT nanocomposites and functionalized MWCNTs were the host materials for silver nanoparticles in the TNC and BNC. The functionalization of MWCNT was achieved by refluxing the MWCNT (0.40 g) with nitric acid (5 M, 50 mL) at 100 °C. The functionalization of MWCNTs reduces the aggregation tendency of MWCNTs in nanocomposites and significantly improves processability. Fourier-transform infrared (FT-IR) spectroscopy confirmed the oxidative functionalization of multiwalled carbon nanotube (MWCNT-COOH). The FT-IR peaks at 1698, 1741, and 3744 cm^{-1} correspond to the carbonyl stretching of aldehyde or keto, carboxyl, and hydrogen-bonded O—H groups, respectively (Figure S1).[57] Polythiophene-functionalized MWCNT (PTCNT-COOH) binary nanocomposites used for the preparation of the ternary silver nanocatalyst contain conducting polythiophene active layers. The forces of attraction between the functionalized MWCNT and polythiophene were predominantly noncovalent attractive forces such as π-interactions, hydrogen bonding, and van der Waals forces. Silver nanoparticles were directly attached to the functionalized multiwalled carbon nanotubes (MWCNT-COOH) in binary silver nanocatalysts (BNC). The preparation, properties, and characterization of PTCNT-COOH 300 Ag (TNC) and MWCNT-COOH Ag (BNC) have been reported by our group.[57] Heterogeneous ternary and binary nanocatalysts were utilized to convert *p*-nitrophenol to *p*-aminophenol in an aqueous medium. The reduction of nitrophenols to aminophenols did not proceed without a catalyst because of the kinetic energy barrier. Therefore, the addition of sodium borohydride to *p*-nitrophenol produces a greenish-yellow solution of the *p*-nitrophenolate ion (Figure 1).[58] On the other hand, in the presence of ternary or binary nanocatalysts, colorless *p*-aminophenolate ions were formed from the greenish-yellow-colored *p*-nitrophenolate ion. The sonication process helps adsorb *p*-nitrophenol to the active sites of nanocatalysts in preparation.[59]

The catalytic conversion of *p*-nitrophenol to *p*-aminophenol was monitored by UV−vis absorbance spectroscopy by noting the decrease in the *p*-nitrophenolate ion peak at 400 nm in successive time intervals after the start of the reaction. Silver nanocatalysts were termed as TNC-0.02, BNC-0.02, TNC-0.04, BNC-0.04, TNC-0.06, BNC-0.06, TNC-0.10, and BNC-0.10, in which the digits represent the concentration of ternary or binary nanocatalysts in mg/mL initially taken in the aqueous P-NP solution for catalytic studies (Table 1 and Table S1). The *p*-nitrophenolate ion peak at 400 nm was produced

https://doi.org/10.1021/acs.iecr.1c01371
Ind. Eng. Chem. Res. 2021, 60, 7050−7064

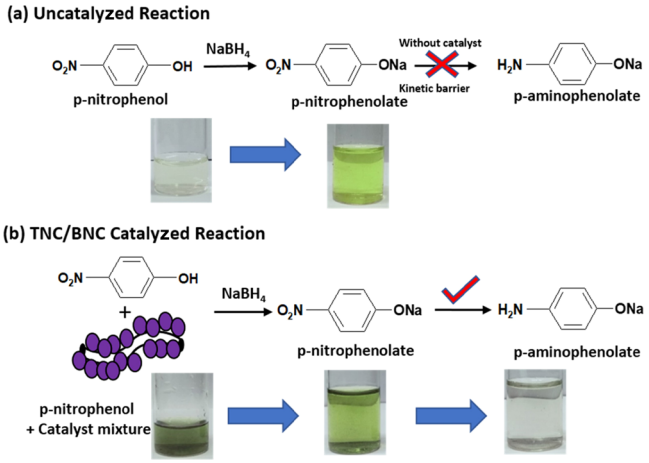

Figure 1. Schematic representation of the *p*-nitrophenol reaction with $NaBH_4$ (a) and TNC/BNC silver nanocatalyst catalyzed reduction of *p*-nitrophenol using $NaBH_4$ (b).

immediately by adding the sodium borohydride solution. As time progresses, the *p*-nitrophenolate ion peak intensity decreases with a concomitant increase of a new peak at 298 nm, corresponding to the *p*-aminophenolate ion (Figure S2).[58] Reaction completion was indicated by the complete suppression of peak at 400 nm. Time-dependent UV−vis absorption spectra using nanocatalyst concentrations TNC-0.06 and BNC-0.06 were recorded (Figure 2A,B). Similarly, the UV−vis absorption spectra for different nanocatalyst concentrations such as TNC-0.02, BNC-0.02, TNC-0.04, BNC-0.04, TNC-0.10, and BNC-0.10 were obtained (Figure S3). The rate constants for this catalytically driven reaction were obtained by plotting ln (A/A_0) against time (Figure 2C for TNC-0.06 catalyzed reaction, Figure 2D for BNC-0.06 catalyzed reaction, and Figure S4 for other concentrations). The reaction follows pseudo-first-order kinetics; therefore, the rate constant can be obtained from the line's slope from the linear regression fit.[60,61] The resultant rate constants were 0.0014, 0.0011, 0.0049, 0.0159, 0.0134, 0.0364, 0.0399, and 0.0540 s^{-1}, respectively, for the catalytic concentrations TNC-0.02, BNC-0.02, TNC-0.04, BNC-0.04, TNC-0.06, BNC-0.06, TNC-0.10, and BNC-0.10. The activity factor (the ratio of the rate constant to the weight of the catalyst used) was also calculated as 35.00, 27.50, 61.25, 198.75, 113.34, 303.34, 199.50, and 270.00 s^{-1} g^{-1} for TNC-0.02, BNC-0.02, TNC-0.04, BNC-0.04, TNC-0.06, BNC-0.06, TNC-0.10, and BNC-0.10, respectively (Table 1). The rate constants of TNC-0.02 and BNC-0.02 were almost equal, but as the nanocatalyst concentrations increase, approximately two to three times greater catalytic activity was obtained for the BNC rather than TNC. The silver nanoparticle-decorated TNC and BNC nanocatalysts rely on electron flow from $NaBH_4$ to *p*-nitrophenol (P-NP) through silver nanoparticles for catalytic reduction. The slow kinetics of the TNC compared with the BNC could be attributed to the electron movement in conducting polythiophene layer.[57,62] Control experiments conducted using silver nanoparticles (Ag NPs) have shown the characteristic surface plasmon resonance peak at 400 nm in freshly prepared conditions (Figure S5). The rate constant for *p*-nitrophenol reduction using Ag NPs (~0.03 mg/mL final concentration) was found ($k = 1.82 \times 10^{-3}$ s^{-1}) to be approximately in the same range that was obtained for TNC-0.02 and BNC-0.02 (Figure S6). In colloidal silver nanoparticles, the surface plasmon resonance peak was overlapped with the nitrophenolate ion peak, making it difficult to note the reaction completion (Figure S6 A). The reduction reaction carried out after the aging of the Ag NP solution for 7 days has shown a slight decrease in the rate constant and settling of nanocolloidal silver nanoparticles (Figure S6C, D). In addition to that, the UV−vis absorption spectra of colloidal silver nanoparticles taken after 7 days lack the surface plasmon resonance peak (Figure S5). Although colloidal silver nanoparticles in freshly prepared conditions act as good catalysts, their aggregation tendency, stability, and recyclability were the major issues. Control experiments conducted using MWCNT-COOH and PTCNT-COOH 300 without silver nanoparticles have not shown catalytic activity (Figure S7). Functionalized MWCNTs/polymers play a vital role as a heterogeneous framework to accommodate silver nanoparticles to prevent agglomeration, rapid oxidation, and leaching.

3.2. Optimization of Nanocatalyst Amount. The optimum nanocatalyst concentrations of the TNC and BNC for reducing *p*-nitrophenol (1.0×10^{-4} M) were selected by plotting A/A_0 against time for different catalyst concentrations (Figure 3A,B). The optimum nanocatalyst concentration has been selected based on the minimum quantity of the nanocatalyst needed to catalyze the reaction at a measurable speed. In general, for all the catalyst concentrations, as the time

Table 1. Name of the Nanocatalyst, Concentrations of Reagents, Amount of Catalyst, Time Taken for Reaction Completion, Rate Constant, and Activity Factor for the Catalytic Reduction of *p*-Nitrophenol

		P-NP		$NaBH_4$					
sl no.	nanocatalyst[a]	conc. (M)	volume (mL)	conc. (M)	volume (mL)	amount of catalyst in 2 mL P-NP solution (mg/mL)	time taken for reaction completion[b] (s)	rate constant[c] (s^{-1})	activity factor[d] (s^{-1} g^{-1})
1	TNC-0.02	1×10^{-4}	2	1×10^{-1}	2	0.02		0.0014	35.00
2	TNC-0.04	1×10^{-4}	2	1×10^{-1}	2	0.04	720	0.0049	61.25
3	TNC-0.06	1×10^{-4}	2	1×10^{-1}	2	0.06	315	0.0134	113.34
4	TNC-0.10	1×10^{-4}	2	1×10^{-1}	2	0.10	180	0.0399	199.50
5	BNC-0.02	1×10^{-4}	2	1×10^{-1}	2	0.02		0.0011	27.50
6	BNC-0.04	1×10^{-4}	2	1×10^{-1}	2	0.04	360	0.0159	198.75
7	BNC-0.06	1×10^{-4}	2	1×10^{-1}	2	0.06	165	0.0364	303.34
8	BNC-0.10	1×10^{-4}	2	1×10^{-1}	2	0.10	45	0.0540	270.00

[a]TNC or BNC taken in different concentrations. [b]Time taken for the disappearance of the nitrophenolate ion peak at 400 nm obtained from UV−visible spectroscopy. [c]The rate constant obtained from the time-dependent UV−vis studies. [d]The ratio rate constant was divided by the weight of the catalyst used.

https://doi.org/10.1021/acs.iecr.1c01371
Ind. Eng. Chem. Res. 2021, 60, 7050−7064

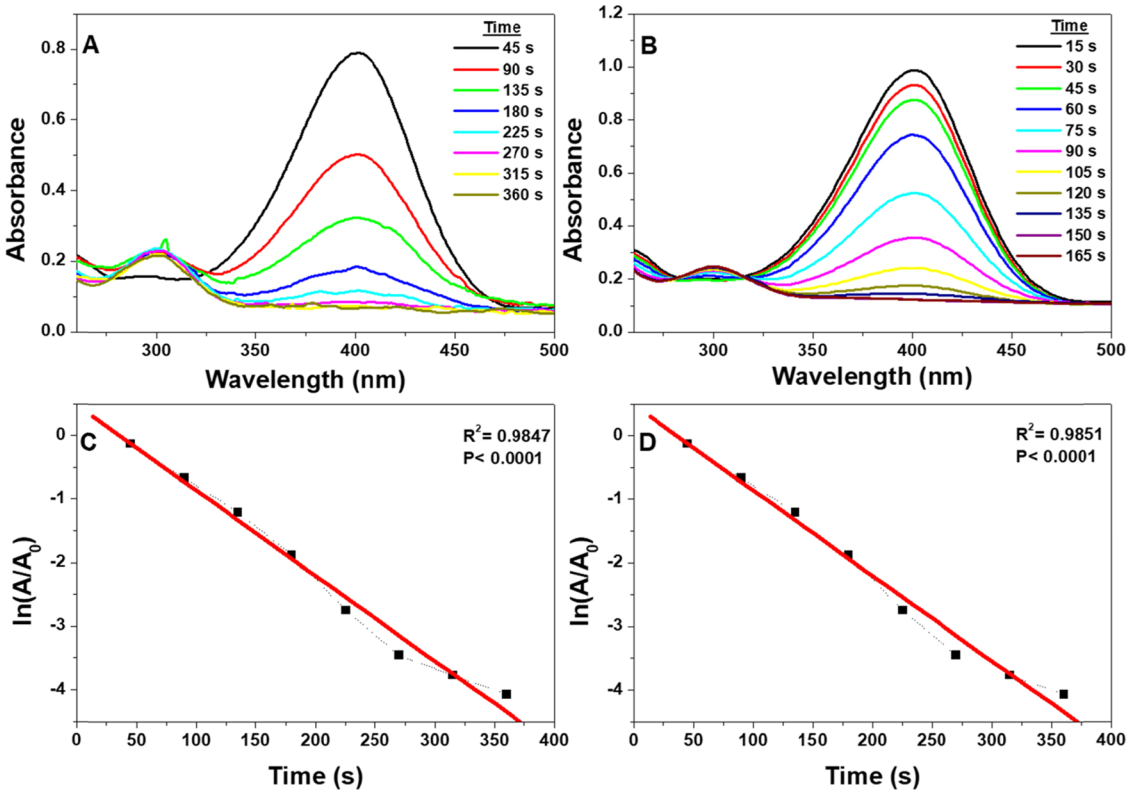

Figure 2. UV−vis absorption spectra of *p*-nitrophenol reduction using catalyst TNC-0.06 (A) and BNC-0.06 (B) in successive time intervals. Linear regression fit of $\ln(A/A_0)$ against time for TNC-0.06 (C) and BNC-0.06 (D) as the nanocatalyst.

increases, the A/A_0 value decreases and reaches a steady minimum in the curve, which corresponds to the completion of the reaction. The time required to reach a steady minimum for TNC-0.04, TNC-0.06, and TNC-0.10 were 550, 315, and 150 s and that for BNC-0.04, BNC-0.06, and BNC-0.10 were 225, 150, and 50 s, respectively. Even though TNC-0.10 and BNC-0.10 have given faster reaction kinetics than TNC-0.06 and BNC-0.06, the latter was selected as optimum catalyst concentrations because of lower catalyst concentrations and measurable speed. By considering other studies reported recently on *p*-nitrophenol reduction using different metal-incorporated nanocomposites, one of the leading catalytic activities was observed in both BNC- and TNC-catalyzed reduction (Table S2 for comparison with other reports).

3.3. Recycling Studies. The recycling studies of the nanocatalysts TNC and BNC were carried out, and the catalytic efficiency in the recycling process was recorded via UV−vis absorption spectroscopy (Figure 4). The TNC was recycled and analyzed for five consecutive cycles and the BNC for six consecutive cycles by fixing the reaction time as 10 min for each cycle. Here, the catalyst was recovered by centrifugation and reused for the next catalytic cycle after washing with water. The catalytic conversion (%) of *p*-nitrophenol to *p*-aminophenol has been determined using the following equation:

$$\text{Conversion (\%)} = \left(1 - \frac{A}{A_0}\right) \text{x } 100$$

where A_0 and A are the absorption maxima of the *p*-nitrophenolate ion at the initial time (t_0) and monitoring time (t), respectively (Figure 4). Catalytic conversion (%) for successive cycles indicated better BNC efficiency than the TNC for six catalytical cycles (Figure 4C,D). TNC has shown a catalytic conversion of 47.56% in the fifth catalytic cycle, whereas the BNC has shown 92.80% conversion in the sixth cycle in identical conditions. The conversion (%) obtained from UV−vis absorbance spectroscopy revealed that the nanocatalyst BNC activates the reaction more than the TNC in multiple cycles. The nanocatalysts recovered from the reaction mixture via centrifugation and washing before subsequent use. Because TNCs are better dispersive than BNCs via sonication, more leaching effect of silver nanoparticles was possible in the former case.

3.4. Elemental Composition and the Morphology of Recycled Nanocatalysts. We have subjected the recycled catalysts to powder XRD studies to trace changes during recycling (Figure 5A,B). The TNC and BNC obtained after the third, sixth, and ninth cycles were named TNC-3RC, TNC-6RC, TNC-9RC, BNC-3RC, BNC-6RC, and BNC-9RC; the digit represents the recycle number. The comparison of the powder XRD patterns of pristine catalysts with recycled catalysts revealed that the intensity of crystalline diffraction peaks corresponding to the silver nanoparticles at 2θ values 38.15°, 44.33°, 64.52°, and 77.46° were decreased considerably after the sixth catalytic cycle (Figure 5A, B).[45] A substantial decrease in the intensity of the diffraction peaks of silver nanoparticles was noticeable on the ninth catalytic cycle of the TNC. The more decrease in the TNC nanocatalyst intensity than the BNC nanocatalyst in higher catalytic cycles was due to the loss of a higher amount of silver nanoparticles during separation, washing, and sonication. The diffraction pattern of BNC-3RC has given crystalline peaks other than silver nanoparticles matching with the crystalline form of sodium metaborate formed as a byproduct from sodium borohydride

https://doi.org/10.1021/acs.iecr.1c01371
Ind. Eng. Chem. Res. 2021, 60, 7050−7064

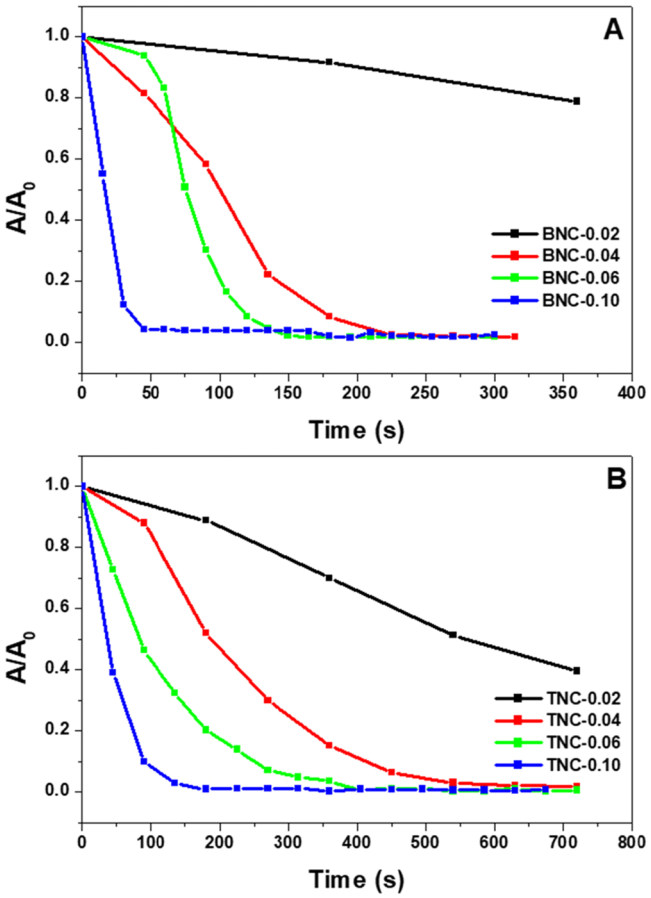

Figure 3. Plot of A/A_0 against time for BNC-catalyzed reactions (A) and TNC-catalyzed reactions (B) for different catalyst concentrations 0.02, 0.04, 0.06, and 0.10 mg/mL taken in the *p*-nitrophenol solution.

(Figure S8).[24,63−65] The inner core structure of the recycled nanocatalysts TNC-3RC and BNC-3RC was determined by XPS (Table S3 and Figure S9). Functionalized MWCNTs contain 94.42 atomic percent of C1s and 5.58 atomic percent of O2s.[57] Recycled binary nanocatalyst BNC-3RC has shown the characteristic peaks of C1s (284.77 eV), O1s (532.47 eV), Na1s (1072.27 eV), Ag3d (374.44 eV), and B1s (192.77 eV) with the atomic percentages of 91.0, 6.6, 1.3, 0.8, and 0.2%, respectively. On the other hand, TNC-3RC has shown the characteristic peaks of C1s (284.78 eV), O1s (532.18 eV), Na1s (1074.08 eV), Ag4s (102.11 eV), B1s (192.77 eV), and S2p (166.47 eV) with the atomic percentages of 76.9, 21.9, 0.3, 0.5, 0.2, and 0.1%, respectively. The higher atomic percentage of C1s in BNC-3RC (91.0%) than TNC-3RC (76.9%) was mainly due to the binary nature, which consists of functionalized MWCNTs and silver nanoparticles only. The presence of sodium metaborate hydrates as a byproduct, intermediate layer of conducting polythiophene, and dopants influence the total atomic percentage of TNC. The atomic composition of the silver atoms of BNC-3RC was higher than TNC-3RC, which matches with the powder XRD data. The decrease in the atomic percentage of silver could be due to the separation of silver nanoparticles in the recycling process.

Silver nanoparticle-embedded pristine TNC and BNC nanocatalysts were subjected to FE-SEM (Figure 5C,D). The TNC contains silver nanoparticles with an average size of 25 ± 5 nm, which exists in a tangled manner on the PTCNT-COOH 300 framework, whereas the BNC contains nanoparticles with an average size of 45 ± 5 nm supported on MWCNT-COOH (Figure S10). The surface morphology and elemental distribution of the recycled catalyst surface have been traced by the SEM and EDX analysis (Figure 6). The FE-SEM images of the recycled nanocatalysts TNC-3RC and BNC-3RC have shown hexagonal crystalline faces over the nanocatalysts (Figure 6A, B). The EDX elemental dot mapping showed a sodium atom percentage of 11.84% in the TNC surface and 14.18% in the BNC surface (Figure 6C, D and Table S3). The oxygen atom % in the same TNC surface was 66.04 atom %, and in BNC, 69.70 atom % (see Figure S11 and Table S3). The presence of sodium atoms and higher oxygen mass percentage from the dot mapping images indicated the formation of sodium metaborate hydrates deposited in the hexagonal phase over the surface of the nanocatalyst. The recycled nanocatalyst TNC-3RC and BNC-3RC contain 1.61 and 1.00 atomic percentages of silver atoms within the EDX analysis limitations (Figure 6E, F and Table S3). A mechanistic scheme of the recycled nanocatalyst (TNC or BNC) represent the after view of the catalytic hydrogenation of *p*-nitrophenol using sodium borohydride (Figure 6G). The TNC and BNC could be reused for many cycles; however, the metaborates trapped in the nanocatalysts could mask the catalytic activity.

3.5. Optimization of the Solvent−Water Mixture for Reduction. The kinetic and mechanistic aspects of BNC- and TNC-catalyzed *p*-nitrophenol reduction were systematically studied using different solvent−water mixtures like glycerol−water, ethylene glycol−water, ethanol−water, and 1,4 dioxane−water. The different catalyst concentrations like TNC-0.03, BNC-0.03, TNC-0.06, and BNC-0.06 were used to reduce *p*-nitrophenol (1.0×10^{-4} M, 5 mL) by the addition of $NaBH_4$ (1.0×10^{-1} M, 5 mL) in the presence of different volume % of solvent−water mixtures. The time of decolorization was noted as the time to complete the reaction. The reaction completion time versus different volume percentages of solvent−water mixtures (5, 10, 20, 30, 40, and 50% v/v) were plotted (Figure 7). The reduction reaction shows faster reaction in the glycerol−water and ethylene glycol−water mixtures, especially in 5−30% volume, and after that, the reaction slows down as the medium's viscosity increases. In the ethanol−water mixture, the reaction rate was slower than that of the abovementioned two mixtures, and the decolorization time increased as the volume percentage of ethanol increases. The least reactivity was observed in the 1,4-dioxane−water mixture, which could be easily understood from the non-availability of active hydrogen in it. Therefore, the order of catalytic reactivity obtained in different solvent−water mixtures was glycerol−water > ethylene glycol−water > ethanol−water >1,4 dioxane−water.

3.6. Optimization of the [P-NP] to [$NaBH_4$] Molar Ratio. The catalytic hydrogenation of *p*-nitrophenol has been conducted by varying the [P-NP] to [$NaBH_4$] molar ratio using TNC-0.06 and BNC-0.06 in 10% v/v glycerol in water (Figure 8A). The different P-NP to $NaBH_4$ molar ratios in water and 10% glycerol−water mixture were 1:50, 1:100, 1:150, 1:250, 1:500, and 1:1000 by fixing the concentration of P-NP solution as 1×10^{-4} M. The decolorization time in catalytic reduction versus the P-NP to $NaBH_4$ molar ratio was plotted (Figure 8A). Decolorization studies have revealed the reaction that follows pseudo-first-order kinetics from the P-NP to $NaBH_4$ molar ratio of 500 onward in water, which reduced to 250 in the glycerol−water mixture.[61] A major disadvantage of reducing nitrophenols with sodium borohydride in water

https://doi.org/10.1021/acs.iecr.1c01371
Ind. Eng. Chem. Res. 2021, 60, 7050−7064

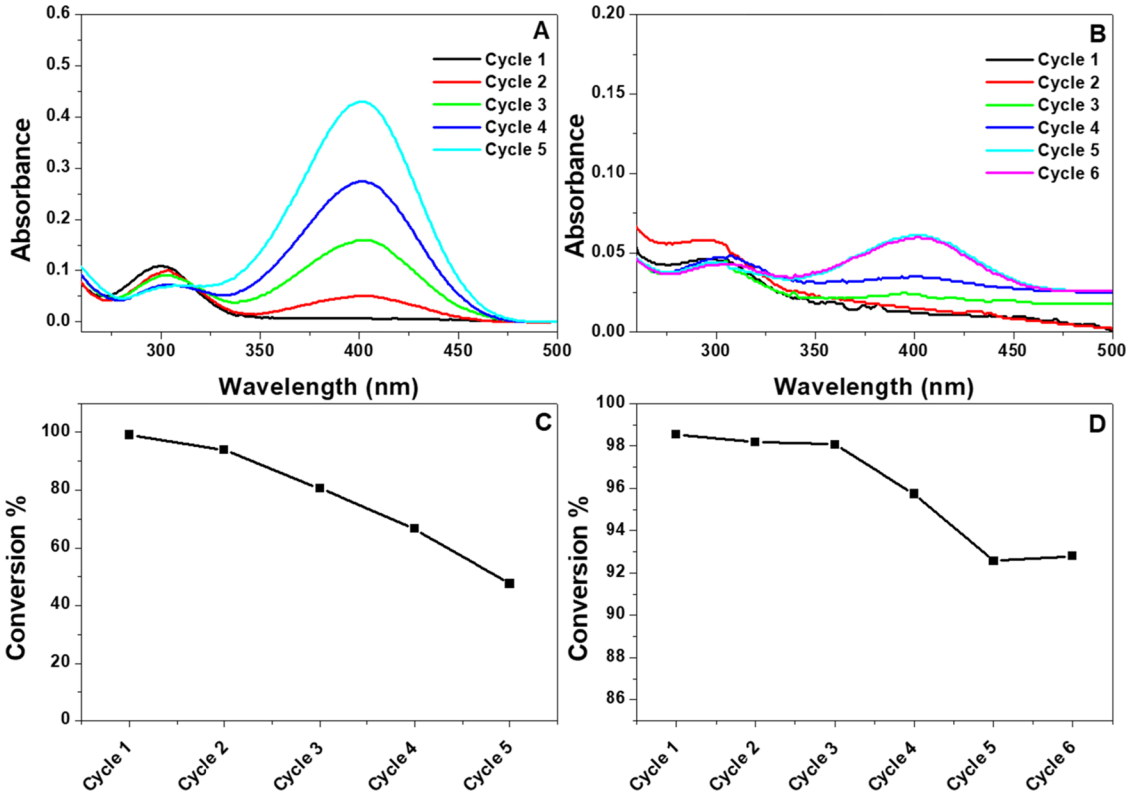

Figure 4. UV−visible absorption spectra of TNC-0.06 catalyzed (A) and BNC-0.06 catalyzed (B) for successive catalytic cycles and catalytic conversion percentage of TNC-0.06 (C) and BNC-0.06 (D) in successive catalytic cycles.

was the excess utilization of $NaBH_4$ to obtain a reasonable reaction rate. Minimizing $NaBH_4$ for *p*-nitrophenol reduction can ensure more economic gain to the synthetic strategy and reduce toxicity effects. The UV−vis absorption spectra were recorded to show the minimum utilization of catalyst with the P-NP to $NaBH_4$ molar ratio of 1:100 in 10% glycerol−water mixture using TNC-0.06, BNC-0.06, and BNC-0.03 catalyst concentrations (Figure 8B, C, and Figure S12). In the presence of a 10% glycerol−water mixture, BNC-0.03 exhibited the same kinetics of BNC-0.06 in water with the P-NP to $NaBH_4$ molar ratio of 1:1000. More interestingly, the catalytic reduction of *p*-nitrophenol was executed with a minimal concentration of the BNC-0.01 catalyst and the P-NP to $NaBH_4$ molar ratio of 1: 200; an excellent activity factor of 936.5 s^{-1} g^{-1} was obtained in a 10% glycerol−water solvent mixture (Figure 8D and Figure S13).

3.7. Proposed Mechanism for Catalytic Reduction. The catalytic reduction mechanism of *p*-nitrophenol using $NaBH_4$ as the reductant remains controversial. The TNC and BNC catalytic performance in different solvent mixtures led us to gain some mechanistic evidence about the hydrogen source used to reduce *p*-nitrophenol. Many possible ways of reduction mechanisms were discussed in the literature.[39,43−48] It was already reported in the literature that the reduction of *p*-nitrophenol did not take place in nonpolar solvents.[39,43,44] However, the involvement of protic solvents using $NaBH_4$ as a reducing agent for *p*-nitrophenol reduction is still inexplicit in its research. In the present experiment, it was noticeable that solvent mixtures like glycerol−water and ethylene glycol−water have shown higher activity than that in water. Other solvent mixtures such as ethanol−water and 1,4-dioxane−water mixtures have shown a lower reduction rate than water, which has given a prime evidence of the active solvent hydrogen involvement in the nitro group's hydrogenation reaction. Sodium borohydride undergoes hydrolysis with water or solvolysis with other solvents containing active hydrogens and produces hydrogen gas.[66] The rate of hydrogen molecule production because of solvolysis in the investigated solvent mixtures at 5−30% v/v follows the order glycerol−water > ethylene glycol−water > water > ethanol−water >1,4-dioxane−water. Three active hydrogens per molecule present in glycerol could be the reason to produce three hydrogen molecules by combining with hydride ions from sodium borohydride. Ethylene glycol has two active hydrogens; water and ethanol have one active hydrogen each, from which a corresponding number of hydrogen molecules could be produced by solvolysis. The ethanol−water mixture has comparably less capacity to form hydrogen molecules than water because $NaBH_4$ exhibited low solubility in ethanol than water. 1,4 dioxane with hydrogens in closed chains was not active as other solvents. The 1,4-dioxane−water mixture, therefore, has a minimal hydrogen production capacity. A direct influence was visible toward active hydrogens' contribution from different solvent molecules to reduce the nitro group. Either sodium borohydride or the active hydrogen-bearing solvent molecules alone could not directly ensure complete nitrophenol hydrogenation. The active hydrogens in solvent molecules combine with the hydride ion from sodium borohydride to produce hydrogen molecules; thereby, the reduction reaction became feasible. The pH of $NaBH_4$, glycerol, and glycerol−$NaBH_4$ mixture in water was checked using a pH meter. The pH of 20% glycerol was 7.2, and that of the $NaBH_4$ solution (1×10^{-1} M) was 10.3. The $NaBH_4$ solution (1×10^{-1} M) was added to the glycerol (25

https://doi.org/10.1021/acs.iecr.1c01371
Ind. Eng. Chem. Res. 2021, 60, 7050−7064

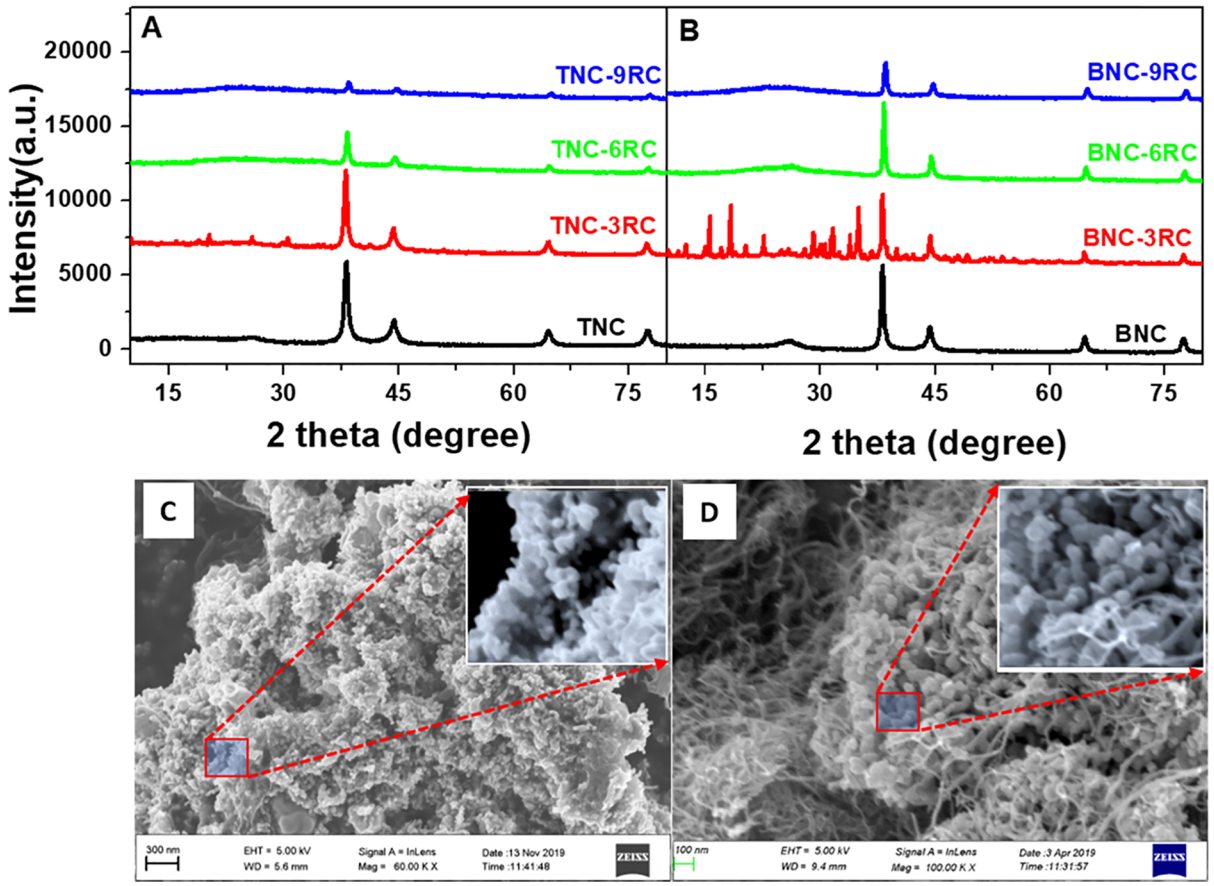

Figure 5. XRD patterns of TNC and recycled TNCs (A), BNC, and recycled BNCs (B) after third, sixth, and ninth catalytic cycles. FE-SEM images of TNC (C) and BNC (D) as pristine nanocatalysts (an enlarged portion is shown in the inset).

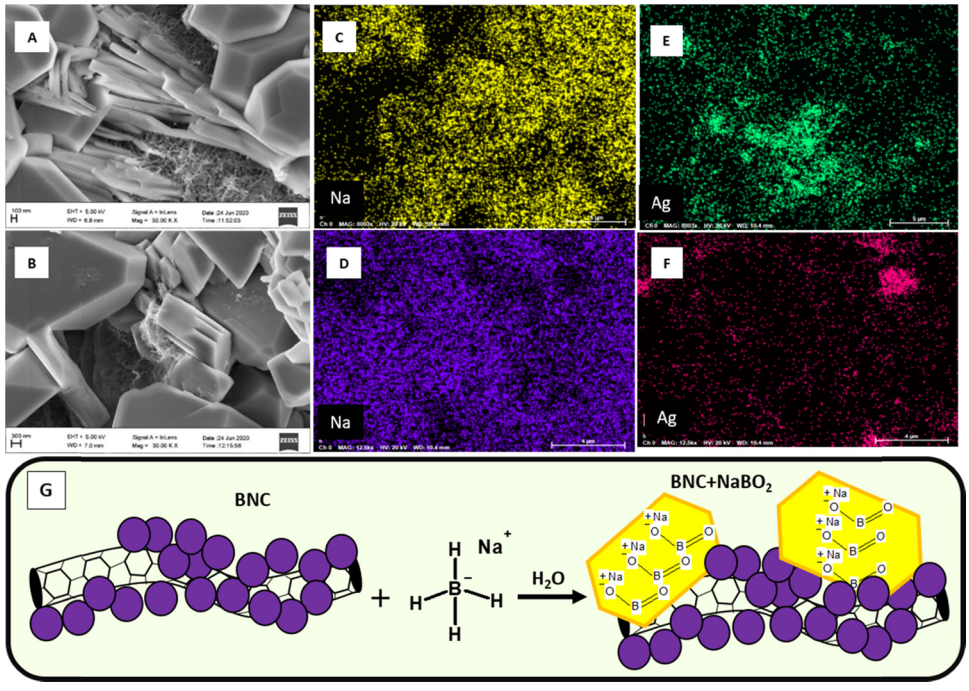

Figure 6. FE-SEM images of TNC-3RC (A) and BNC-3RC (B), EDX color mapping of sodium in TNC-3RC (C), sodium in BNC-3RC (D), silver in TNC-3RC (E), and silver in BNC-3RC (F). Schematic representation of metaborate byproduct over a recycled catalyst (G).

mL, 20%) solution, and the pH of the corresponding solution mixtures was checked with 2 mL addition. A graph was plotted with the volume of the $NaBH_4$ solution added against the pH of the reaction mixture (Figure S14). The reaction mixture pH

https://doi.org/10.1021/acs.iecr.1c01371
Ind. Eng. Chem. Res. 2021, 60, 7050−7064

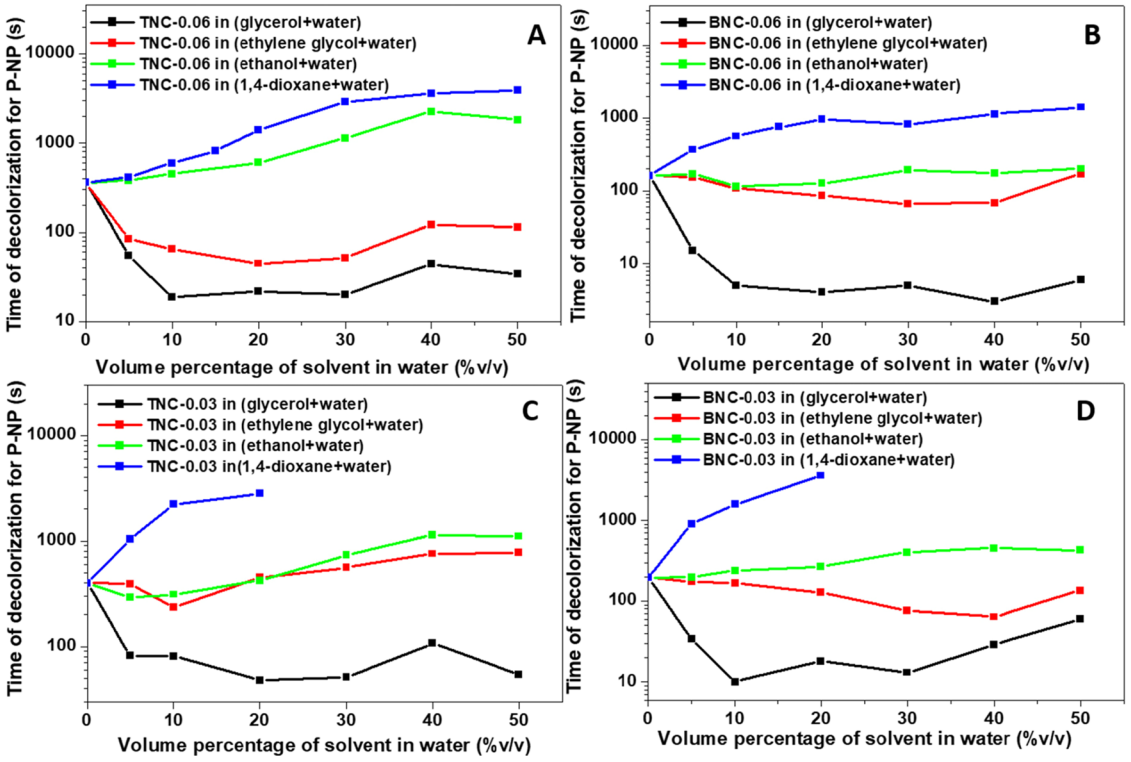

Figure 7. Time of decolorization taken against different volume percentages of the solvent−water mixture with PNP: $NaBH_4$ molar ratio 1:1000 using (A) TNC-0.06, (B) BNC-0.06, (C) TNC-0.03, and (D) BNC-0.03 as the catalyst.

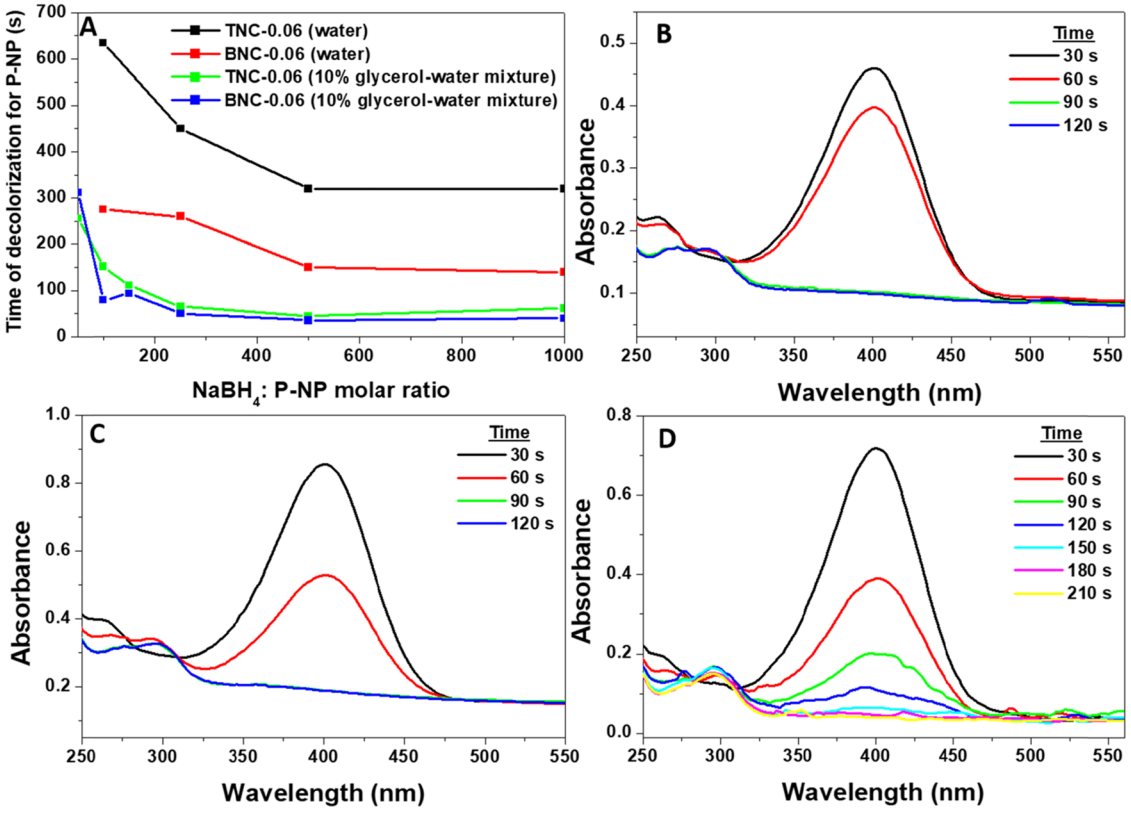

Figure 8. Time of decolorization against different $NaBH_4$: P-NP molar ratios in water and 10% glycerol−water mixture using TNC-0.06 and BNC-0.06 (A), UV−vis absorption spectra of reduction of *p*-nitrophenol using catalyst TNC-0.06 (PNP: $NaBH_4$ molar ratio 1:100) (B), using BNC-0.06 (PNP: $NaBH_4$ molar ratio 1:100) (C) and BNC-0.01 (PNP: $NaBH_4$ molar ratio 1:200) in 10% glycerol−water solvent mixture (D).

https://doi.org/10.1021/acs.iecr.1c01371
Ind. Eng. Chem. Res. 2021, 60, 7050−7064

increased by $NaBH_4$ addition and reached a pH of 9.5 by adding 50 mL of the 1×10^{-1} M $NaBH_4$ solution. The reduction mainly happened in alkaline conditions; therefore, the production of hydrogen molecules by the reaction of $NaBH_4$ with active solvent hydrogen was the major factor rather than the change in pH. The dielectric constant of solvent mixtures on the reduction rate was studied.[67−69] The solvent mixtures used in the present study have lower dielectric constants than water; however, the reaction rates in the glycerol−water mixture and ethylene glycol−water mixture exhibited a higher reaction rate than that in water. A plausible mechanism has been shown in Figure 9. Two probable reasons

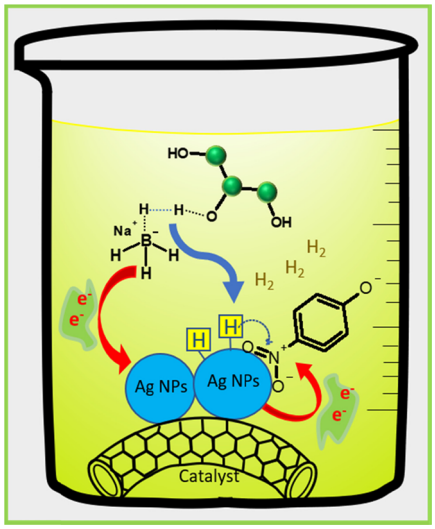

Figure 9. Mechanism of active solvent hydrogen-enhanced green catalytic reduction of *p*-nitrophenol using $NaBH_4$ in 10% glycerol−water mixture.

could be attributed here for the catalytic hydrogenation of the nitro group by the silver nanocatalyst. Active hydrogen species could be produced via the solvolysis of the glycerol−water mixture with sodium borohydride, which has the primary role in enhancing the catalytic reduction rate.[21,70,71] This reactive hydrogen species gets adsorbed on the catalyst's surface to convert *p*-nitrophenol to *p*-aminophenol.[21,72] The second possibility was the conventional way of catalytic hydrogenation by the hydrogen molecules produced in the solvolysis.[40,47] Faster kinetics of the *p*-nitrophenol reduction in the glycerol−water mixture using $NaBH_4$ as the reductant indicates that the major path could be the highly energetically reactive hydrogen species-involved reduction.

3.8. Effect of Dispersion Stability on Catalytic Activity. The catalytic reduction of *p*-nitrophenol was carried out in different concentrations of *p*-nitrophenol from 1.0×10^{-2} to 1.0×10^{-4} M. For this study, five times higher nanocatalyst amount was taken to reduce the *p*-nitrophenol solution for observing the aggregation behavior during the catalytic reaction. The decolorization time increases with an increase in the concentration of *p*-nitrophenol for a fixed amount of $NaBH_4$ and catalyst. We could note from the photographs that the BNC underwent faster aggregation in the reaction mixture, whereas the TNC exhibited a more stable dispersion in the reaction medium (Figure S15). A graph was plotted using the ratio t_{nd}/t_{1d} versus the different P-NP concentrations. t_{nd} was the time taken for decolorization for the *n*th higher concentration of P-NP, and t_{1d} is the time taken for decolorization in the initial concentration of P-NP (Figure S16). The BNC has two to three times more activity than the TNC at lower P-NP concentrations; however, as the P-NP concentration increases, the t_{nd}/t_{1d} ratio was better maintained for TNC than BNC. The reason for the poor performance of BNC is the rapid aggregation and consequent settling of BNC. The aggregation of the nanocatalyst could decrease the effective surface area, thereby hiding the active catalytic sites for catalytic reduction.[62a]

3.9. Relative Yield and Industrial-Scale Reduction of *p*-Nitrophenol. The relative yield of the *p*-aminophenolate ion was obtained from the calibration curve of the known concentrations of *p*-aminophenolate (Figure 10A). Different *p*-aminophenol solution concentrations from 5.0×10^{-4} to 1.0×10^{-7} M were prepared. For measuring the absorbance of the *p*-aminophenolate ion, a freshly prepared $NaBH_4$ solution (10 mL, 1.0×10^{-1} M) was added to each concentration of *p*-aminophenol (Figure 10A and Figure S17). The absorbance of the *p*-aminophenolate ion from the nanocatalytic reduction of *p*-nitrophenol (1.0×10^{-4} M) was almost matching with the known concentration of aminophenol, indicating complete conversion (Figure 10B). The synthetic utility of the amino phenolate product has been substantiated by the diazotization reaction (inset of Figure 10B). The catalytical conversion of *p*-nitrophenol to *p*-aminophenol in 10% glycerol−water mixture using the minimum P-NP to $NaBH_4$ molar ratio (1:25), by taking nanocatalyst concentration BNC-0.18, could be extended to high-concentration scale up for industrial catalysis (near the saturation limit of *p*-nitrophenol in water). Reaction completion was observed in green reaction conditions within 1 h (Figure 10C for photographs). The reaction mixture's UV−vis absorption spectra taken after 1 h of reaction time have shown a peak at 298 nm corresponding to the *p*-aminophenolate ion (Figure 10D). The absence of the *p*-nitrophenolate peak at 400 nm and the existence of a single peak at 298 nm validated the complete reduction of *p*-nitrophenol to *p*-aminophenolate. Aminophenol's widespread applications in commercial and industrial fields demand the bulk-scale hydrogenation of nitrophenol, which can be successfully prepared using heterogeneous silver nanocatalysts and by the utilization of a less volume percentage of glycerol.[73,74]

3.10. Antibacterial Activity. Antibacterial activity studies of the nanocomposite TNC have been carried out on *E. coli*, a frequently used model organism in life science research.[75,76] Silver nanoparticles act as good antibacterial agents depending on the particle size and shape.[25,26] TNCs have been taken for the antibacterial study in different doses because of their capability to maintain appreciably stable dispersion for a longer time. The antibacterial activity and minimum inhibitory concentration (MIC) of nanocomposites have been studied using the tube dilution method. Different concentrations of TNC 1×10^{-1}, 5×10^{-1}, 1, 5, 10, 20, 30, 40, 80, 120, and 160 μg/mL were prepared. The mixtures were dispersed in a boiling tube for 10 min, and 50 μL of actively growing *E. coli* culture was used as the inoculum for all tubes. It was incubated in a thermal shaker overnight at 37 °C. Microbial growth in the liquid medium was characterized by increased turbidity, and for that, incubation tubes were examined under bright light. The white turbidity resulting from *E. coli* bacterial growth was almost absent in the medium above the 10 μg/mL concentration of TNC (Figure 11A). The result indicates that TNC exhibits good antibacterial activity against gram-

https://doi.org/10.1021/acs.iecr.1c01371
Ind. Eng. Chem. Res. 2021, 60, 7050−7064

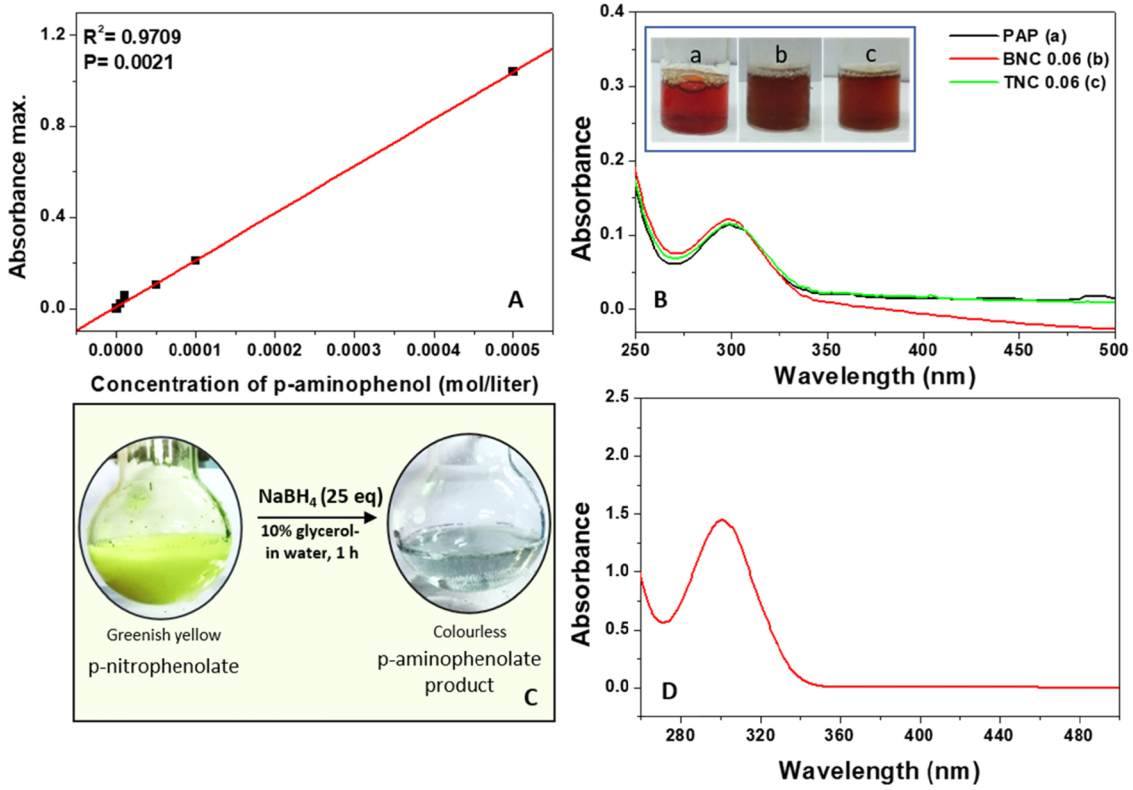

Figure 10. Calibration plot of *p*-aminophenol in different concentrations (1×10^{-7}–5×10^{-4} M) (A), UV–vis absorption spectra of the standard solution of *p*-aminophenolate ion, *p*-aminophenolate obtained from catalytic reduction using TNC-0.06 and BNC-0.06 (in 1×10^{-4} M) (B), reduction of *p*-nitrophenol in the concentrated solution (10 mL, 15 g/L) using P-NP: $NaBH_4$ molar ratio of 1:25 and BNC-0.18 (0.18 mg/mL) in 10% glycerol–water mixture (C), and UV–vis spectrum *p*-aminophenolate produced by bulk concentration-scale reduction.

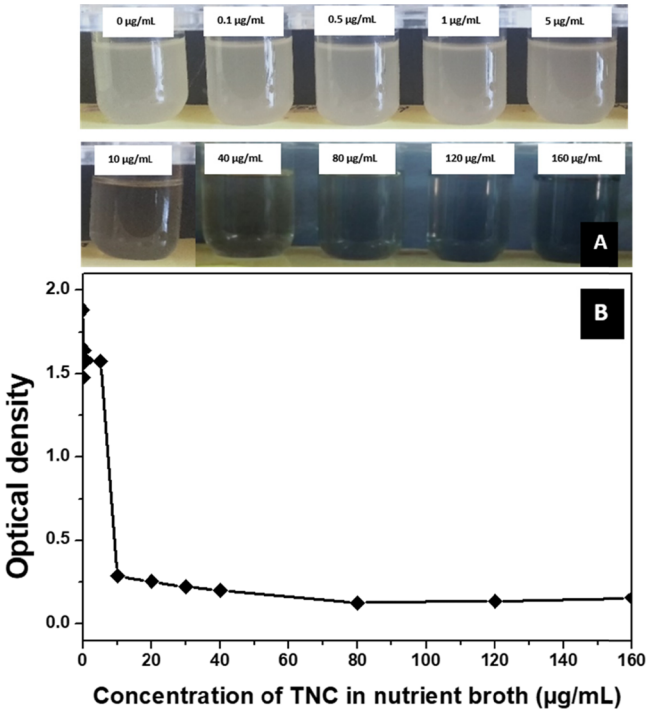

Figure 11. Photographs of mixtures of *E. coli* bacteria culture with different concentrations of TNC taken after overnight incubation (A). Plot of optical density versus the concentration of TNC for the antibacterial study at 660 nm (B).

negative *E. coli* bacteria. The quantitative assessment of antibacterial activity was done by measuring optical density at 660 nm using a UV–vis double beam spectrophotometer. A graph was plotted taking optical density versus the concentration of TNC used for antibacterial studies (Figure 11B). The nutrient broth–TNC mixture has high optical density for concentrations between 5×10^{-1} and 10 μg/mL because of the bacterial growth; however, at 10 μg/mL of the nanocatalyst, the optical density considerably suppressed because of the inhibition to the growth of the bacterial culture. The MIC of TNC was estimated as 10 μg/mL, comparable with the reference range of commercial antimicrobial agents.[77,78] The TNC with one-dimensional nanostructure in which silver nanoparticles are attached to MWCNTs via a less cytotoxic polythiophene layer.[49,57,62a] Silver nanoparticles attached to the nanocomposite can be biocidal by physicochemical interactions with bacterial cells.[26] The comparison study of the antibacterial activity of MWCNT-COOH, PTCNT-COOH 300, Ag nanoparticles colloidal solution (Ag NPs), BNC, and TNC against *E. coli* bacteria was carried out using lactose broth (lactose broth was selected here to repeat antibacterial activity in another medium) (Figure S18 and Supporting Information for the procedure). TNC has shown a higher antibacterial activity against *E. coli* bacteria in the dosage of 10 μg/mL and above. Silver nanoparticles in the dosage of 10 μg/mL show a lower antibacterial activity than TNC, which may be due to the aggregation effect of some of the Ag NPs during the incubation period. BNC exhibited a lower antibacterial activity than that of TNC because of the incapability to maintain stable dispersion for the overnight incubation period. MWCNT-

https://doi.org/10.1021/acs.iecr.1c01371
Ind. Eng. Chem. Res. 2021, 60, 7050–7064

COOH and PTCNT-COOH 300 have no observable antibacterial activity in the range 10−30 μg/mL. The well-dispersed state of TNC made them highly competent for bacterial inactivation because good dispersion provides more nanosurface active sites for interacting with bacteria.[48] The properties of excellent water dispersibility and recovering nature could be combined with the high antibacterial activity of TNC; therefore, it could find unique applications in different fields such as water disinfection, medical fields, textile industries.[48,49]

4. CONCLUSIONS

We have studied the active solvent hydrogen-enhanced catalytic hydrogenation of *p*-nitrophenol using $NaBH_4$ with two types of heterogeneous silver nanocatalysts. Polymer-supported silver nanoparticle-embedded functionalized MWCNT (TNC) and silver nanoparticles directly-embedded functionalized MWCNT nanocomposites (BNC). The BNC was found to exhibit higher catalytic performance than TNC in the conversion percentage and recycling efficiency. Separate control experiments using the Ag NPs solution, MWCNT-COOH, and PTCNT-COOH revealed that Ag NPs act as a catalyst for reduction and functionalized MWCNT-COOH acts as a supporting framework for stabilizing silver nanoparticles and polythiophene layers to improve the dispersing nature of the nanocomposites. Comparative studies of the kinetics of *p*-nitrophenol reduction in water and different solvent−water mixtures such as 1,4-dioxane−water, ethanol−water, ethylene glycol−water, and glycerol−water have been demonstrated. The 10% glycerol−water mixture was an efficient green solvent mixture for the enhanced rate of reduction. By utilizing the minimum amount of catalyst (0.005 mg/mL) and P-NP to $NaBH_4$ molar ratio 1:200 in a glycerol−water mixture, a fast reduction of *p*-nitrophenol was obtained with an activity factor of 936.50 s^{-1} g^{-1}. A plausible mechanism of the hydrogen source for converting the nitro group to amino group by the solvolysis of $NaBH_4$ in a protic solvent has been proposed. Active hydrogens present in the solvent molecules were showing a direct impact on accelerating P-NP reduction using $NaBH_4$. The high concentration scale preparation of *p*-aminophenol using a simple green organic reaction set up with a modest reaction time of 1 h has been achieved by reducing *p*-nitrophenol (1.08×10^{-1} M) using catalyst concentrations BNC-0.18 and $NaBH_4$ (2.69 M). The TNC could also act as an efficient antibacterial agent against the widely used model organism *E. coli* with a minimum concentration of 10 μg/mL.

■ ASSOCIATED CONTENT

Supporting Information

The Supporting Information is available free of charge at https://pubs.acs.org/doi/10.1021/acs.iecr.1c01371.

Procedures of catalytic studies, tables of catalytic reaction parameters, literature comparison, and elemental analysis. FT-IR spectra of MWCNTs and MWCNT-COOH. UV−vis absorption spectra and kinetic plots using TNC-0.02, BNC-0.02, TNC-0.04, BNC-0.04, TNC-0.10, BNC-0.10, and control experiments. Size calculation of silver nanoparticles in catalysts. Characterizations of metaborate byproduct of catalytic reduction. The change in pH of the glycerol−water mixture (20%) with $NaBH_4$ addition. UV−vis absorption spectra of BNC-0.03 and the linear relationship plot using BNC-0.01. Photographs and catalytic reduction in different concentrations of P-NP. UV−vis absorption plot of *p*-aminophenol. Comparison study of antibacterial activity in lactose broth (PDF)

■ AUTHOR INFORMATION

Corresponding Author

M. Jinish Antony − *Research and P.G. Department of Chemistry, Centre for Sustainable Chemistry, St. Thomas College (Autonomous Under University of Calicut), Thrissur, Kerala 680 001, India;* orcid.org/0000-0003-2639-1006; Email: jinish06@yahoo.co.in

Authors

T. S. Swathy − *Research and P.G. Department of Chemistry, Centre for Sustainable Chemistry, St. Thomas College (Autonomous Under University of Calicut), Thrissur, Kerala 680 001, India*

Naijil George − *Department of Biotechnology, St. Joseph's College (Autonomous Under University of Calicut), Irinjalakuda, Thrissur, Kerala 680 121, India*

Complete contact information is available at: https://pubs.acs.org/10.1021/acs.iecr.1c01371

Notes

The authors declare no competing financial interest.

■ ACKNOWLEDGMENTS

We acknowledge DST for FIST facilities and UGC for CPE-funded central instrumentation facilities in St. Thomas' College (autonomous), Thrissur. We acknowledge Ms. Kavya Raj K. for the technical support for antibacterial activity studies at St. Joseph's College, Irinjalakuda. We also acknowledge the Optoelectronic Device Laboratory, Department of Physics, CUSAT, Cochin, for providing FE-SEM/EDX facility, and NIIST, Trivandrum, for providing XPS analysis facility. T.S.S. acknowledges university grants commission (UGC), New Delhi, for JRF fellowship. M.J.A. gratefully acknowledges his doctoral mentor Dr. M. Jayakannan, Professor IISER, Pune, for his guidance and support.

■ REFERENCES

(1) Heveling, J. Heterogeneous Catalytic Chemistry by Example of Industrial Applications. *J. Chem. Educ.* **2012**, *89*, 1530.

(2) Liu, L.; Corma, A. Metal Catalysts for Heterogeneous Catalysis: From Single Atoms to Nanoclusters and Nanoparticles. *Chem. Rev.* **2018**, *118*, 4981.

(3) Mizuno, N.; Misono, M. Heterogeneous Catalysis. *Chem. Rev.* **1998**, *98*, 199.

(4) Chandrasekhar, V.; Athimoolam, A. New Hybrid Inorganic-Organic Polymers as Supports for Heterogeneous Catalysis: A Novel Pd(0) Metalated Cyclophosphazene-Containing Polymer as an Efficient Heterogeneous Catalyst for the Heck Reaction. *Org. Lett.* **2002**, *4*, 2113.

(5) Friend, C. M.; Xu, B. Heterogeneous Catalysis: A Central Science for a Sustainable Future. *Acc. Chem. Res.* **2017**, *50*, 517.

(6) Zhou, Y.; Huang, R.; Ding, F.; Brittain, A. D.; Liu, J.; Zhang, M.; Xiao, M.; Meng, Y.; Sun, L. Sulfonic Acid-Functionalized α-Zirconium Phosphate Single-Layer Nanosheets as a Strong Solid Acid for Heterogeneous Catalysis Applications. *ACS Appl. Mater. Interfaces* **2014**, *6*, 7417.

(7) Shi, J. On the Synergetic Catalytic Effect in Heterogeneous Nanocomposite Catalysts. *Chem. Rev.* **2013**, *113*, 2139.

(8) Liu, X.; Wen, X.; Hoffmann, R. Surface Activation of Transition Metal Nanoparticles for Heterogeneous Catalysis: What We Can Learn from Molecular Dynamics. *ACS Catal.* **2018**, *8*, 3365.
(9) Zhao, P.; Feng, X.; Huang, D.; Yang, G.; Astruc, D. Basic Concepts and Recent Advances in Nitrophenol Reduction by Gold- and Other Transition Metal Nanoparticles. *Coord. Chem. Rev.* **2015**, *287*, 114.
(10) Campelo, J. M.; Luna, D.; Luque, R.; Marinas, J. M.; Romero, A. A. Sustainable Preparation of Supported Metal Nanoparticles and Their Applications in Catalysis. *ChemSusChem* **2009**, *2*, 18.
(11) Astruc, D. Introduction: Nanoparticles in Catalysis. *Chem. Rev.* **2020**, *120*, 461.
(12) Deshmukh, S. P.; Dhodamani, A. G.; Patil, S. M.; Mullani, S. B.; More, K. V.; Delekar, S. D. Interfacially Interactive Ternary Silver-Supported Polyaniline/Multiwalled Carbon Nanotube Nanocomposites for Catalytic and Antibacterial Activity. *ACS Omega* **2020**, *5*, 219.
(13) Alshehri, S. M.; Almuqati, T.; Almuqati, N.; Al-Farraj, E.; Alhokbany, N.; Ahamad, T. Chitosan Based Polymer Matrix with Silver Nanoparticles Decorated Multiwalled Carbon Nanotubes for Catalytic Reduction of 4-Nitrophenol. *Carbohydr. Polym.* **2016**, *151*, 135.
(14) Ahmad, S.; Yang, C.; Xie, W.; Deng, Z.; Zhang, H.; Zhao, Y.; Su, X. Molten Salt-Templated Synthesis of Ternary NiS−$NiCo_2O_4$@C Composites as High Performance Catalysts for 4-Nitro Phenol Reduction and Supercapacitor. *Carbon* **2020**, *158*, 912.
(15) Nariya, P.; Das, M.; Shukla, F.; Thakore, S. Synthesis of Magnetic Silver Cyclodextrin Nanocomposite as Catalyst for Reduction of Nitro Aromatics and Organic Dyes. *J. Mol. Liq.* **2020**, *300*, No. 112279.
(16) Yang, X.; Jiang, X.; Bashir, M. S.; Kong, X. Z. Preparation of Highly Uniform Polyurethane Microspheres by Precipitation Polymerization and Pd Immobilization on Their Surface and Their Catalytic Activity in 4-Nitrophenol Reduction and Dye Degradation. *Ind. Eng. Chem. Res.* **2020**, *59*, 2998.
(17) Kibar, G.; Dinç, D. Ş. Ö. In-Situ Growth of Ag on Mussel-Inspired Polydopamine@poly(M-POSS) Hybrid Nanoparticles and Their Catalytic Activity. *J. Environ. Chem. Eng.* **2019**, *7*, No. 103435.
(18) Liao, G.; Zhao, W.; Li, Q.; Pang, Q.; Xu, Z. Novel Poly (Acrylic Acid)-Modified Tourmaline/Silver Composites for Adsorption Removal of Cu(II) Ions and Catalytic Reduction of Methylene Blue in Water. *Chem. Lett.* **2017**, *46*, 1631.
(19) Liao, G.; Fang, J.; Li, Q.; Li, S.; Xu, Z.; Fang, B. Ag-Based Nanocomposites: Synthesis and Applications in Catalysis. *Nanoscale* **2019**, *11*, 7062.
(20) Liao, G.; Li, Q.; Zhao, W.; Pang, Q.; Gao, H.; Xu, Z. In-Situ Construction of Novel Silver Nanoparticle Decorated Polymeric Spheres as Highly Active and Stable Catalysts for Reduction of Methylene Blue Dye. *Appl. Catal. A Gen.* **2018**, *549*, 102.
(21) Liao, G.; Gong, Y.; Zhong, L.; Fang, J.; Zhang, L.; Xu, Z.; Gao, H.; Fang, B. Unlocking the Door to Highly Efficient Ag-Based Nanoparticles Catalysts for $NaBH_4$-Assisted Nitrophenol Reduction. *Nano Res.* **2019**, *12*, 2407.
(22) Sarkar, A. K.; Saha, A.; Midya, L.; Banerjee, C.; Mandre, N.; Panda, A. B.; Pal, S. Cross-Linked Biopolymer Stabilized Exfoliated Titanate Nanosheet-Supported AgNPs: A Green Sustainable Ternary Nanocomposite Hydrogel for Catalytic and Antimicrobial Activity. *ACS Sustainable Chem. Eng.* **2017**, *5*, 1881.
(23) Liu, R.; Hou, Y.; Jiang, S.; Nie, B. Ag(I)-Hived Fullerene Microcube as an Enhanced Catalytic Substrate for the Reduction of 4-Nitrophenol and the Photodegradation of Orange G Dye. *Langmuir* **2020**, *36*, 5236.
(24) Kolya, H.; Kuila, T.; Kim, N. H.; Lee, J. H. Bioinspired Silver Nanoparticles/Reduced Graphene Oxide Nanocomposites for Catalytic Reduction of 4-Nitrophenol, Organic Dyes and Act as Energy Storage Electrode Material. *Compos. Part B Eng.* **2019**, *173*, No. 106924.
(25) González, A. L.; Noguez, C.; Beránek, J.; Barnard, A. S. Size, Shape, Stability, and Color of Plasmonic Silver Nanoparticles. *J. Phys. Chem. C* **2014**, *118*, 9128.
(26) Tejamaya, M.; Römer, I.; Merrifield, R. C.; Lead, J. R. Stability of Citrate, PVP, and PEG Coated Silver Nanoparticles in Ecotoxicology Media. *Environ. Sci. Technol.* **2012**, *46*, 7011.
(27) Astruc, D.; Lu, F.; Aranzaes, J. R. Nanoparticles as Recyclable Catalysts: The Frontier between Homogeneous and Heterogeneous Catalysis. *Angew. Chem. - Int. Ed.* **2005**, *44*, 7852.
(28) Yu, B.; Han, B.; Jiang, X.; Zhou, C.; Xia, K.; Gao, Q.; Wu, J. Toward High Activity and Durability: An Oxygen-Rich Boron Nitride-Supported Au Nanoparticles for 4-Nitrophenol Hydrogenation. *J. Phys. Chem. C* **2019**, *123*, 10389.
(29) Shifrina, Z. B.; Matveeva, V. G.; Bronstein, L. M. Role of Polymer Structures in Catalysis by Transition Metal and Metal Oxide Nanoparticle Composites. *Chem. Rev.* **2020**, *120*, 1350.
(30) Bilalis, P.; Katsigiannopoulos, D.; Avgeropoulos, A.; Sakellariou, G. Non-Covalent Functionalization of Carbon Nanotubes with Polymers. *RSC Adv.* **2014**, *4*, 2911.
(31) Zahed, B.; Hosseini-Monfared, H. A Comparative Study of Silver-Graphene Oxide Nanocomposites as a Recyclable Catalyst for the Aerobic Oxidation of Benzyl Alcohol: Support Effect. *Appl. Surf. Sci.* **2015**, *328*, 536.
(32) Baruah, B.; Gabriel, G. J.; Akbashev, M. J.; Booher, M. E. Facile Synthesis of Silver Nanoparticles Stabilized by Cationic Polynorbornenes and Their Catalytic Activity in 4-Nitrophenol reduction. *Langmuir* **2013**, *29*, 4225.
(33) Gangu, K. K.; Maddila, S.; Jonnalagadda, S. B. A Review on Novel Composites of MWCNTs Mediated Semiconducting Materials as Photocatalysts in Water Treatment. *Sci. Total Environ.* **2019**, *646*, 1398.
(34) Liao, G.; Gong, Y.; Zhang, L.; Gao, H.; Yang, G. J.; Fang, B. Semiconductor Polymeric Graphitic Carbon Nitride Photocatalysts: The "Holy Grail" for the Photocatalytic Hydrogen Evolution Reaction under Visible Light. *Energy Environ. Sci.* **2019**, *12*, 2080.
(35) Ali, G. A. M.; Megiel, E.; Cieciórski, P.; Thalji, M. R.; Romański, J.; Algarni, H.; Chong, K. F. Ferrocene Functionalized Multi-Walled Carbon Nanotubes as Supercapacitor Electrodes. *J. Mol. Liq.* **2020**, *318*, No. 114064.
(36) Zhan, W.; Yu, S.; Gao, L.; Wang, F.; Fu, X.; Sui, G.; Yang, X. Bioinspired Assembly of Carbon Nanotube into Graphene Aerogel with "Cabbagelike" Hierarchical Porous Structure for Highly Efficient Organic Pollutants Cleanup. *ACS Appl. Mater. Interfaces* **2018**, *10*, 1093.
(37) Liu, T.; Sun, Y.; Jiang, B.; Guo, W.; Qin, W.; Xie, Y.; Zhao, B.; Zhao, L.; Liang, Z.; Jiang, L. Pd Nanoparticle-Decorated 3D-Printed Hierarchically Porous TiO_2 Scaffolds for the Efficient Reduction of a Highly Concentrated 4-Nitrophenol Solution. *ACS Appl. Mater. Interfaces* **2020**, *12*, 28100.
(38) Kästner, C.; Thünemann, A. F. Catalytic Reduction of 4-Nitrophenol Using Silver Nanoparticles with Adjustable Activity. *Langmuir* **2016**, *32*, 7383.
(39) Li, Z.; He, M.; Wen, Y.; Zhang, X.; Hu, M.; Li, R.; Liu, J.; Chu, J.; Ma, Z.; Xing, X.; Yu, C.; Wei, Z.; Li, Y. Highly Monodisperse Cu−Sn Alloy Nanoplates for Efficient Nitrophenol Reduction Reaction via Promotion Effect of Tin. *Inorg. Chem.* **2020**, *59*, 1522.
(40) Scholten, J. D.; Leal, B. C.; Dupont, J. Transition Metal Nanoparticle Catalysis in Ionic Liquids. *ACS Catal.* **2012**, *2*, 184.
(41) Shirin, S.; Roy, S.; Rao, A.; Pillai, P. P. Accelerated Reduction of 4-Nitrophenol: Bridging Interaction Outplays Reducing Power in the Model Nanoparticle-Catalyzed Reaction. *J. Phys. Chem. C* **2020**, *124*, 19157.
(42) Neal, R. D.; Hughes, R. A.; Sapkota, P.; Ptasinska, S.; Neretina, S. Effect of Nanoparticle Ligands on 4-Nitrophenol Reduction: Reaction Rate, Induction Time, and Ligand Desorption. *ACS Catal.* **2020**, *10*, 10040.
(43) Zhao, Y.; Li, R.; Jiang, P.; Zhang, K.; Dong, Y.; Xie, W. Mechanistic Study of Catalytic Hydride Reduction of −NO2 to −NH2 Using Isotopic Solvent and Reducer: The Real Hydrogen Source. *J. Phys. Chem. C* **2019**, *123*, 15582.
(44) Fountoulaki, S.; Daikopoulou, V.; Gkizis, P. L.; Tamiolakis, I.; Armatas, G. S.; Lykakis, I. N. Mechanistic Studies of the Reduction of

https://doi.org/10.1021/acs.iecr.1c01371
Ind. Eng. Chem. Res. 2021, 60, 7050−7064

Nitroarenes by NaBH4 or Hydrosilanes Catalyzed by Supported Gold Nanoparticles. *ACS Catal.* **2014**, *4*, 3504.
(45) Das, R.; Sypu, V. S.; Paumo, H. K.; Bhaumik, M.; Maharaj, V.; Maity, A. Silver Decorated Magnetic Nanocomposite (Fe_3O_4@PPy-MAA/Ag) as Highly Active Catalyst towards Reduction of 4-Nitrophenol and Toxic Organic Dyes. *Appl. Catal. B Environ.* **2019**, *244*, 546.
(46) Narayanan, R. K.; Devaki, S. J. Brawny Silver-Hydrogel Based Nanocatalyst for Reduction of Nitrophenols: Studies on Kinetics and Mechanism. *Ind. Eng. Chem. Res.* **2015**, *54*, 1197.
(47) Mogudi, B. M.; Ncube, P.; Meijboom, R. Catalytic Activity of Mesoporous Cobalt Oxides with Controlled Porosity and Crystallite Sizes: Evaluation Using the Reduction of 4-Nitrophenol. *Appl. Catal. B Environ.* **2016**, *198*, 74.
(48) Krystosiak, P.; Tomaszewski, W.; Megiel, E. High-Density Polystyrene-Grafted Silver Nanoparticles and Their Use in the Preparation of Nanocomposites with Antibacterial Properties. *J. Colloid Interface Sci.* **2017**, *498*, 9.
(49) Zako, T.; Sakono, M.; Kobayashi, T.; Sörgjerd, K.; Nilsson, K. P. R.; Hammarström, P.; Lindgren, M.; Maeda, M. Cell Interaction Study of Amyloid by Using Luminescent Conjugated Polythiophene: Implication That Amyloid Cytotoxicity Is Correlated with Prolonged Cellular Binding. *ChemBioChem* **2012**, *13*, 358.
(50) Moreira, T.; Laia, C. A. T.; Zangoli, M.; Antunes, M.; Di Maria, F.; De Monte, S.; Liscio, F.; Parola, A. J.; Barbarella, G. Semicrystalline Polythiophene-Based Nanoparticles Deposited from Water on Flexible PET/ITO Substrates as a Sustainable Approach toward Long-Lasting Solid-State Electrochromic Devices. *ACS Appl. Polym. Mater.* **2020**, *2*, 3301.
(51) Moghayedi, M.; Goharshadi, E. K.; Ghazvini, K.; Ahmadzadeh, H.; Ranjbaran, L.; Masoudi, R.; Ludwig, R. Kinetics and Mechanism of Antibacterial Activity and Cytotoxicity of Ag-RGO Nanocomposite. *Colloids Surf.* **2017**, *159*, 366.
(52) Murugan, E.; Vimala, G. Effective Functionalization of Multiwalled Carbon Nanotube with Amphiphilic Poly(Propyleneimine) Dendrimer Carrying Silver Nanoparticles for Better Dispersability and Antimicrobial Activity. *J. Colloid Interface Sci.* **2011**, *357*, 354.
(53) Liao, G.; He, F.; Li, Q.; Zhong, L.; Zhao, R.; Che, H.; Gao, H.; Fang, B. Emerging Graphitic Carbon Nitride-Based Materials for Biomedical Applications. *Prog. Mater. Sci.* **2020**, *112*, No. 100666.
(54) Liao, G.; Gong, Y.; Yi, C.; Xu, Z. Soluble, Antibaterial, and Anticorrosion Studies of Sulfonated Polystyrene/Polyaniline/Silver Nanocomposites Prepared with the Sulfonated Polystyrene Template. *Chinese J. Chem.* **2017**, *35*, 1157.
(55) Marambio-Jones, C.; Hoek, E. M. V. A Review of the Antibacterial Effects of Silver Nanomaterials and Potential Implications for Human Health and the Environment. *J. Nanopart. Res.* **2010**, *12*, 1531.
(56) Gozdziewska, M.; Cichowicz, G.; Markowska, K.; Zawada, K.; Megiel, E. Nitroxide-Coated Silver Nanoparticles: Synthesis, Surface Physicochemistry and Antibacterial Activity. *RSC Adv.* **2015**, *5*, 58403.
(57) Swathy, T. S.; Jinish, A. M. Tangled Silver Nanoparticles Embedded Polythiophene-Functionalized Multiwalled Carbon Nanotube Nanocomposites with Remarkable Electrical and Thermal Properties. *Polymer* **2020**, *189*, No. 122171.
(58) Wang, Z.; Xu, C.; Gao, G.; Li, X. Facile Synthesis of Well-Dispersed Pd-Graphene Nanohybrids and Their Catalytic Properties in 4-Nitrophenol reduction. *RSC Adv.* **2014**, *4*, 13644.
(59) Feng, Y.; Yin, J.; Liu, S.; Wang, Y.; Li, B.; Jiao, T. Facile Synthesis of Ag/Pd Nanoparticle - Loaded Poly(Ethylene Imine) Composite Hydrogels with Highly Efficient Catalytic Reduction of 4-Nitrophenol. *ACS Omega* **2020**, *5*, 3725.
(60) Liao, G.; Chen, J.; Zeng, W.; Yu, C.; Yi, C.; Xu, Z. Facile Preparation of Uniform Nanocomposite Spheres with Loading Silver Nanoparticles on Polystyrene-Methyl Acrylic Acid Spheres for Catalytic Reduction of 4-Nitrophenol. *J. Phys. Chem. C* **2016**, *120*, 25935.
(61) Gu, S.; Wunder, S.; Lu, Y.; Ballauff, M.; Fenger, R.; Rademann, K.; Jaquet, B.; Zaccone, A. Kinetic Analysis of the Catalytic Reduction of 4-Nitrophenol by Metallic Nanoparticles. *J. Phys. Chem. C* **2014**, *118*, 18618.
(62) (a) Kaloni, T. P.; Giesbrecht, P. K.; Schreckenbach, G.; Freund, M. S. Polythiophene: From Fundamental Perspectives to Applications. *Chem. Mater.* **2017**, *29*, 10248. (b) Swathy, T. S.; Jose, M. A.; Antony, M. J. AOT Assisted Preparation of Ordered, Conducting and Dispersible Core-Shell Nanostructured Polythiophene − MWCNT Nanocomposites. *Polymer* **2016**, *103*, 206. (c) Jose, M. A.; Varghese, S.; Antony, M. J. In situ chemical oxidative polymerization for ordered conducting polythiophene nanostructures in presence of dioctyl sodium sulfosuccinate. *Indian J. Chem.* **2016**, *55A*, 292.
(63) Pozun, Z. D.; Rodenbusch, S. E.; Keller, E.; Tran, K.; Tang, W.; Stevenson, K. J.; Henkelman, G. A Systematic Investigation of *p*-Nitrophenol Reduction by Bimetallic Dendrimer Encapsulated Nanoparticles. *J. Phys. Chem. C* **2013**, *117*, 7598.
(64) Ortiz-Quiñonez, J. L.; Pal, U. Borohydride-Assisted Surface Activation of $Co_3O_4/CoFe_2O_4$ Composite and Its Catalytic Activity for 4-Nitrophenol reduction. *ACS Omega* **2019**, *4*, 10129.
(65) Chen, W.; Ouyang, L. Z.; Liu, J. W.; Yao, X. D.; Wang, H.; Liu, Z. W.; Zhu, M. Hydrolysis and Regeneration of Sodium Borohydride (NaBH4) − A Combination of Hydrogen Production and Storage. *J. Power Sources* **2017**, *359*, 400.
(66) (a) Schlesinger, H. I.; Brown, H. C.; Finholt, A. E.; Gilbreath, J. R.; Hoekstra, H. R.; Hyde, E. K. Sodium Borohydride, Its Hydrolysis and Its Use as a Reducing Agent and in the Generation of Hydrogen. *J. Am. Chem. Soc.* **1953**, *75*, 215. (b) Alhokbany, N.; Ahama, T.; Ruksana; Naushad, M.; Alshehri, S. M. AgNPs Embedded N- Doped Highly Porous Carbon Derived from Chitosan Based Hydrogel as Catalysts for the reduction of 4-Nitrophenol. *Compos. Part B Eng.* **2019**, *173*, No. 106950. (c) Åkerlöf, G. Dielectric Constants of Some Organic Solvent-Water Mixtures at Various Temperatures. *J. Am. Chem. Soc.* **1932**, *54*, 4125.
(67) Mohsen-Nia, M.; Amiri, H.; Jazi, B. Dielectric Constants of Water, Methanol, Ethanol, Butanol and Acetone: Measurement and Computational Study. *J. Solution Chem.* **2010**, *39*, 701.
(68) Jouyban, A.; Soltanpour, S. Prediction of Dielectric Constants of Binary Solvents at Various Temperatures. *J. Chem. Eng. Data* **2010**, *55*, 2951.
(69) Brown, H. C.; Mead, E. J.; Rao, B. C. S. A Study of Solvents for Sodium Borohydride and the Effect of Solvent and the Metal Ion on Borohydride Reductions. *J. Am. Chem. Soc.* **1955**, *77*, 6209.
(70) Wang, W.; Niu, J.; Yang, Z. An Efficient Reduction of Unsaturated Bonds and Halogen-Containing Groups by Nascent Hydrogen over Raney Ni Catalyst. *J. Hazard. Mater.* **2020**, *389*, No. 121912.
(71) Song, J.; Huang, Z. F.; Pan, L.; Li, K.; Zhang, X.; Wang, L.; Zou, J. J. Review on Selective Hydrogenation of Nitroarene by Catalytic, Photocatalytic and Electrocatalytic Reactions. *Appl. Catal. B Environ.* **2018**, *227*, 386.
(72) Clarke, C. J.; Tu, W. C.; Levers, O.; Bröhl, A.; Hallett, J. P. Green and Sustainable Solvents in Chemical Processes. *Chem. Rev.* **2018**, *118*, 747.
(73) Kitanosono, T.; Masuda, K.; Xu, P.; Kobayashi, S. Catalytic Organic Reactions in Water toward Sustainable Society. *Chem. Rev.* **2018**, *118*, 679.
(74) Xiu, Z. M.; Zhang, Q. B.; Puppala, H. L.; Colvin, V. L.; Alvarez, P. J. J. Negligible Particle-Specific Antibacterial Activity of Silver Nanoparticles. *Nano Lett.* **2012**, *12*, 4271.
(75) Andrews, J. M. Determination of Minimum Inhibitory Concentrations. *J. Antimicrob. Chemother.* **2001**, *48*, 5.
(76) Ramalingam, B.; Parandhaman, T.; Das, S. K. Antibacterial Effects of Biosynthesized Silver Nanoparticles on Surface Ultrastructure and Nanomechanical Properties of Gram-Negative Bacteria Viz. Escherichia Coli and Pseudomonas Aeruginosa. *ACS Appl. Mater. Interfaces* **2016**, *8*, 4963.
(77) Antony, R.; Marimuthu, R.; Murugavel, R. Bimetallic Nanoparticles Anchored on Core-Shell Support as an Easily

https://doi.org/10.1021/acs.iecr.1c01371
Ind. Eng. Chem. Res. 2021, 60, 7050−7064

Recoverable and Reusable Catalytic System for Efficient Nitroarene Reduction. *ACS Omega* **2019**, *4*, 9241.
(78) Deshmukh, S. P.; Patil, S. M.; Mullani, S. B.; Delekar, S. D. Silver Nanoparticles as an Effective Disinfectant: A Review. *Mater. Sci. Eng. C* **2019**, *97*, 954.

https://doi.org/10.1021/acs.iecr.1c01371
Ind. Eng. Chem. Res. 2021, 60, 7050−7064